Draft version April 12, 2019
Typeset using LaTeX twocolumn style in AASTeX62

Improving Damped Random Walk parameters for SDSS Stripe82 Quasars with baseline extension with PanStarrs1 data.

Krzysztof L. Suberlak,[1] Željko Ivezić,[1] and Chelsea MacLeod[2]

[1] Department of Astronomy
University of Washington
Seattle, WA 98195, USA
[2] Harvard Smithsonian Center for Astrophysics
60 Garden St, Cambridge, MA 02138, USA

(Received January 1, 2019; Revised January 17, 2019; Accepted February 1, 2019)

Submitted to ApJ

ABSTRACT

1. INTRODUCTION

Quasars are variable. Their light curves have been successfully described using the Damped Random Walk (DRW) model (Kelly et al. 2009; MacLeod et al. 2010; Kozłowski et al. 2010; Zu et al. 2011; Kasliwal et al. 2015). The origin of variability is debated, with thermal origin being the favorite explanation (Kelly et al. 2013), connected to the inhomogeneity of the accretion disk (Dexter & Agol 2011), or even magnetically elevated disks (Dexter & Begelman 2019).

The DRW parameters have been linked to the physical quasar properties: MacLeod et al. (2010) found correlations of the characteristic timescale and variability amplitude to the black hole mass, and quasar luminosity.

Inherent variability, and modelling it as a DRW, is also a reliable way to distinguish quasars from stars based on optical photometry (MacLeod et al. 2011). In that case the fit biases are less important than the fact that DRW timescale and amplitude for QSO are order of magnitude different from stars (MacLeod et al. 2011). It is especially useful for selecting quasars in the intermediate redshift range that could not be easily identified by color-color diagrams (Sesar et al. 2007; Yang et al. 2017).

Accurate QSO population studies are important for measurement of Quasar Luminosity Function, and variability has been used before to increase the completeness of quasar selection (Ross et al. 2013; Palanque-Delabrouille et al. 2013; AlSayyad 2016; McGreer et al. 2013, 2018).

Corresponding author: Krzysztof Suberlak
suberlak@uw.edu

Because DRW is a stochastic process, two light curves with identical DRW parameters will not look identical. However, once can still fit the available data with the DRW model and recover fit parameters. It has been found (eg. MacLeod et al. (2011); Kozłowski et al. (2010); Kozłowski, Szymon (2017)) that regardless of method, we can most reliably recover input parameters if we use the longest light curve baseline possible. A rule of thumb is that the light curve has to be at least ten times longer than the recovered timescale. We confirm this observation with simulations of DRW light curves spanning a variety of ratios of input timescale to light curve lenght.

The light curve baseline is the key in an unbiased recovery of light curve parameters. As it has been 8 years since MacLeod et al. (2010) have published their research, we can now benefit from additional data from other surveys that have observed the same quasars since. We show how combining the SDSS data with CRTS, PTF , PS1, and simulated LSST data, decreases the bias in recovered parameters. Thus with added data, extending the baseline on average by 50%, we revisit correlations studied by MacLeod et al. (2010). We confirm the general trends, and provide forecast for improvement with the advent of ZTF, LSST. Extended baseline is the advantage that is not afforded by studies only using single survey data (eg. Hernitschek et al. (2016)

2. METHODS

2.1. *DRW as a Gaussian Process*

DRW (OrnsteinUhlenbeck process) can be understood as a member of a class of Gaussian Processes (GP). Each GP is described by a kernel - a covariance function that contains a measure of correlation between two points

x_n, x_m, separted by Δt_{nm}. For the DRW process, the kernel is

$$k(\Delta t_{nm}) = a \exp\left(-\Delta t_{tm}/\tau\right) \quad (1)$$
$$= \sigma^2 \exp\left(-\Delta t_{tm}/\tau\right) \quad (2)$$
$$= \sigma^2 ACF(\Delta t_{tm}) \quad (3)$$

Here a or σ^2 is an amplitude of correlation decay as a function of t_{tm}, while τ is the characteristic timescale over which correlation drops by $1/e$. For a DRW, the correlation function $k(\Delta t_{nm})$ is also related to the autocorrelation function ACF.

Related to $k(\Delta t_{nm})$ is the structure function of the DRW process (see MacLeod et al. (2012); Bauer et al. (2009); Graham et al. (2015) for an overview) , which expresses the rms of magnitude differences Δm as a function of temporal separation Δt, is :

$$SF(\Delta t) = SF_{\infty}(1 - \exp\left(-|\Delta t|/\tau\right))^{1/2} \quad (4)$$

where SF_{∞} is the asymptotic value of SF for large time lags. It is known that for QSOs SF follows approximately power law, $SF \propto \Delta t^{\beta}$, and it levels out for large Δt) (see MacLeod et al. (2012)). Note that $SF_{\infty} = \sqrt{2}\sigma$ in the above.

To estimate the DRW parameters and fit simulated or real data we employ Celerite - a new fast GP modelling tool(Foreman-Mackey et al. 2017). Combined with the DRW kernel this is similar to the method used by Rybicki & Press (1992); Kozłowski et al. (2010); MacLeod et al. (2010) - like in previous work, we use a prior on σ and τ uniform in log space. The main difference is that rather than adopting the Maximum A-Posteriori (MAP) as the 'best-fit' value for sought parameters, we find the expectation value of the marginalized log posterior. If the posterior space was a 2D Gaussian in σ, τ space, the expectation value would coincide with the maximum of the log posterior. However, due to non-Gaussian shape of the log posterior, we find that the expectation value is a better estimate of σ and τ rather than MAP.

2.2. *The impact of light curve baseline*

Kozłowski, Szymon (2017) reports that we cannot trust any results of DRW fitting unless the light curve length is at least ten times longer than the characteristic timescale. We confirm these generic trends by repeating Kozłowski, Szymon (2017) simulation setup. We model 10 000 DRW light curves with fixed length (baseline) $t_{exp} = 8$ years, $SF_{\infty} = 0.2$ mag, but with different input timescales. We parametrize the ratio of timescale to baseline by $\rho = \tau/t_{exp}$. Given that the baselines for all light curves are fixed, by selecting different input τ we probe a logarithmic grid in $\rho \in \{0.01 : 15\}$. For each of 100 distinct values of ρ we perform 100 light curve realizations.

To simulate observational conditions we add to the true underlying signal $s(t)$ a noise offset, $n(t)$. Like Kozłowski, Szymon (2017), we assume $n(t)$ to be drawn from a Gaussian distribution $\mathcal{N}(0, \sigma(t))$ with a width $\sigma(t)$, corresponding to the photometric uncertainty at the given epoch, $e(t)$) :

$$y(t) = s(t) + n(t) \quad (5)$$

The $s(t)$ is found by iterating over the array of time steps t. At each step, we draw a point from a Gaussian distribution, for which the mean and standard deviation are re-calculated at each timestep. Starting at t_0, the signal is equal to the mean magnitude, $s_0 = m$. After a timestep $\Delta t_i = t_{i+1} - t_i$, the signal s_{i+1} is drawn from $\mathcal{N}(loc, stdev)$, with :

$$loc = s_i e^{-r} + m\left(1 - e^{-r}\right) \quad (6)$$

and

$$stdev^2 = 0.5\,\mathrm{SF}_{\infty}^2\left(1 - e^{-2r}\right) \quad (7)$$

where $r = \Delta t_i/\tau$, τ is the damping timescale, SF_{∞} is the variability amplitude , and m the mean magnitude. This follows the formalizm in Kelly et al. (2009) (eqs. A4 and A5) as well as in MacLeod et al. (2010) (Sec. 2.2), and is equivalent to the setup of Kozłowski, Szymon (2017).

We adopt SDSS S82-like cadence with N=60 epochs, or OGLE-III like cadence with N=445 epochs. The errors were set by the adopted mean magnitudes, $r = 17$ and $I = 18$, as in Kozłowski, Szymon (2017) :

$$\sigma^2_{SDSS} = 0.013^2 + \exp\left(2(r - 23.36)\right) \quad (8)$$
$$\sigma^2_{OGLE} = 0.004^2 + \exp\left(1.63(I - 22.55)\right) \quad (9)$$

Fig 1 shows that as stipulated in Kozłowski, Szymon (2017), the recovered ρ becomes meaningless ('unconstrained') if the available baseline is not at least ten times longer than the underlying timescale. It also means that by extending the baseline we can move from the biased region to the unbiased regime.

Encouraged by this result, we extend the baselines of quasar light curves, and revisit relations studied by MacLeod et al. (2011) and Hernitschek et al. (2016).

3. DATA

3.1. *Surveys*

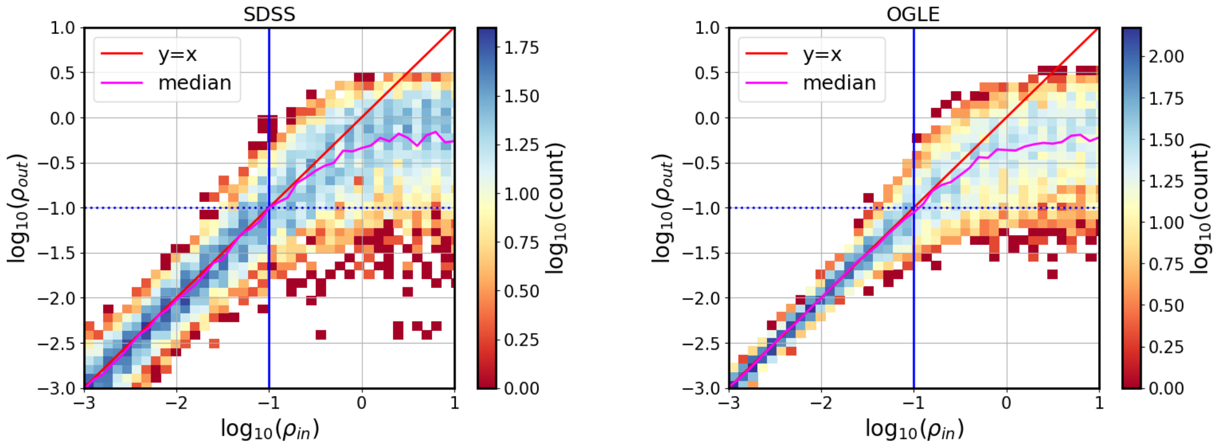

Figure 1. Probing the parameter space of $\rho = \tau/t_{exp}$, with a simulation of 10 000 light curves : 100 light curves per each of 100 ρ values spaced uniformly in logarithmic space between $\rho \in \{0.01 : 15\}$. Thus with the baseline t_{exp} set to 8 years, we sample a range of 100 input timescales, as in Kozłowski, Szymon (2017). Left panel shows the SDSS-like cadence with N=60 points, and the right panel OGLE-like cadence with N=445 points. The dotted horizontal and solid vertical lines represent $\rho = 0.1$, i.e. the baseline is ten times longer than considered timescale. The diagonal line is $y = x$, i.e. the line that would be followed if the recovered ρ (τ) was exactly the same as the input ρ (τ).

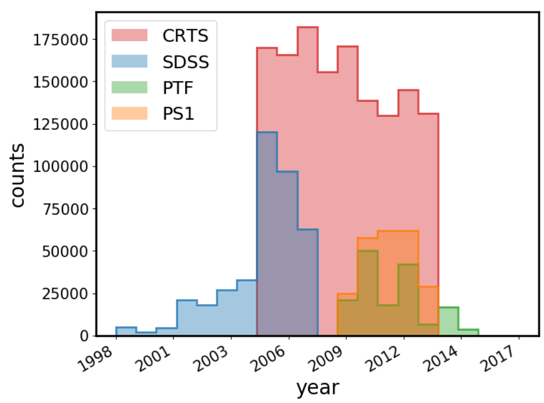

Figure 2. Raw photometric measurements for quasars in Stripe 82 from SDSS(r), PS1(gri), PTF(gR), CRTS(V).

We focus on data pertaining to a 290 deg^2 region of southern sky, repeatedly observed by the SDSS between 1998 and 2008. Originally aimed at supernova discovery, objects in this area, known as Stripe82 (S82), were re-observed on average 60 times (see MacLeod et al. 2012 Sec. 2.2 for overview, and Annis et al. 2014 for details) . Availability of well-calibrated (Ivezić et al. 2007), long-baseline light curves spurred variability research (see Sesar et al. 2007). The catalog prepared by (Schneider et al. 2008) as part of DR9 contains 9258 spectroscopically confirmed quasars.

We extend the SDSS light curves with PanSTARRS (PS1) (Chambers 2011; Flewelling 2018), CRTS (Drake et al. 2009), and PTF (Rau et al. 2009). We find 9248 PS1 matches, 6455 PTF matches, and 7737 CRTS matches to SDSS S82 quasars. There are 6444 quasars with SDSS-PS1-PTF-CRTS data. Fig. 2 shows the distribution of raw epochs, and Fig 3 the baseline coverage of various surveys. Each survey uses a unique set of bandpasses and cadences : SDSS light curves contain near-simultaneous $\{u, g, r, i, z\}_{SDSS}$, and the other are non-simultaneous : $\{g, r, i, z, y\}_{PS1}$, $\{g, R\}_{PTF}$, V_{CRTS}.

3.2. *Photometric offsets*

To utilize all data we define a common 'target' bandpass. SDSS r band is closest to PS1 r, PTFr, CRTSV. For this reason we translate photometry from nearby filters ($\{g, R\}_{PTF}$, $\{g, r, i\}_{PS1}$, V_{CRTS}) to the 'master' r_{SDSS} band.

With two photometric systems, eg. SDSS(ugriz), and PS1(grizy), we can find offsets (or color terms) from one to another. Consider SDSS as target system, PS1 as the auxiliary system, so that we find offsets from PS1 to SDSS. This amounts to creating 'synthetic' SDSS bands from PS1, using the SDSS color to spread the stellar locus. More generally, we would always use the color of the target system :

$$r_{PS1} - r_{SDSS} = f(SDSS(g - i)) \tag{10}$$

the function is a polynomial fitted to the stellar locus on the plot of $SDSS(g - i)$ vs $r_{PS1} - r_{SDSS}$. We use $SDSS(g - i)$ because is provides a larger wavelength baseline than $(g - r)$.

Note that there are other possible choices for the target band and the intermediate color to spread the stellar locus. For instance, rewriting the above as $m - s = f(x)$, Tonry et al. (2012) derived offsets from SDSS to PS1

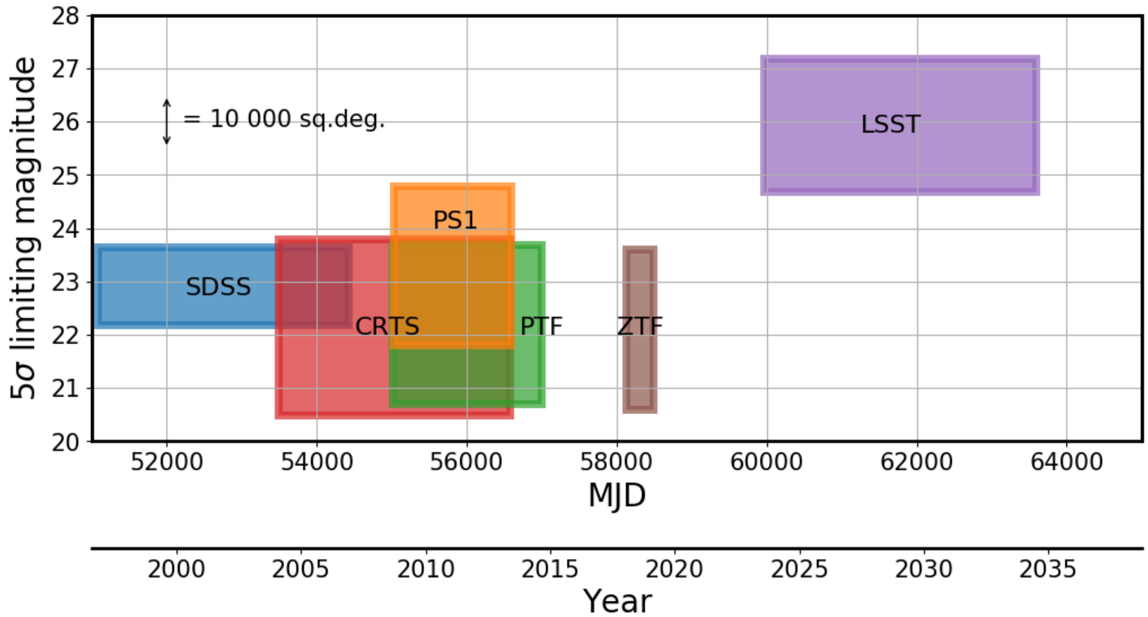

Figure 3. An illustration of survey baseline, sky area covered, and depth. The width of each rectangle corresponds to the extent of light curves available (or simulated) for Stripe 82 quasars for each survey. For SDSS this means DR7; for CRTS DR2, PS1 DR2, PTF DR2, ZTF year 2018, and LSST the full 10-year survey. The lower edge of each rectangle corresponds to the 5σ limiting magnitude (SDSS r, PS1 r, PTF R, ZTF r, LSST r, CRTS V). The vertical extent corresponds to the total survey area (for SDSS, up to and including DR15). Note how PS1 and PTF extend the baseline of SDSS by approximately 50%, and how inclusion of LSST triples the SDSS baseline. For reference, the area covered by LSST is 25000 sq.deg., which corresponds to 60% of the sky. The whole sky has an area of 4π steradians (41253 sq.deg.).

using $x = \mathrm{SDSS}(g-r)$, $m = PS1\{g,r,i,z,y\}$, and $s = \mathrm{SDSS}(r)$.

Since quasars occupy a blue region in the color-color diagram (Fig. 4), we calculate photometric offsets specifically for this region of the spectrum. We only show the color-magnitude diagrams for PS1 offsets (Fig. 5) since we choose not to include CRTS and PTF data in the final sample.

The offsets used to make combined r-band light curves are shown in Table 1

4. SIMULATION : LESSONS LEARNED

Having established in Sec. 2.2 that extending the light curve baseline improves the recovery of input DRW parameters, we combine SDSS light curves with PS1 data. We first consider the theoretical improvement in the fit, simulating DRW light curves for which we select SDSS-PS1 , or SDSS-only sections. Then we fit the real data with DRW model, and divide by (1+z) to study the timescales in rest frame.

We simulate the DRW using the real cadences and errors corresponding to sections of combined light curves (SDSS,PS1,CRTS,PTF), including the portion corresponding to the predicted LSST and ZTF contribution. For LSST segment we assumed a cadence of 50 epochs per year, for 10 years (between 2023-2033), and magnitude-dependent photometric uncertainty from Sec. 3.5 in LSST Science Collaboration et al. (2009):

$$\sigma_{LSST}(m)^2 = \sigma_{sys}^2 + \sigma_{rand}^2 \ (\mathrm{mag})^2 \tag{11}$$

$$\sigma_{rand}^2 = (0.04-\gamma)x + \gamma x^2 \tag{12}$$

$$x = 10^{0.4(m-m_5)} \tag{13}$$

with $\sigma_{sys} = 0.005$, $\gamma = 0.039$, $m_5 = 24.7$ (see Table 3.2 therein).

For the ZTF segment (the 2018 data that covers Stripe82, to be released May 9 2019), we have assumed 120 observations in ZTFg and ZTFr, every three days, with error structure derived from ZTF light curves. We fitted the functional form described above to estimate the ZTF photometric uncertainty (see Fig. 6)

For all light curves we assumed $\tau = 575$ days, $SF_\infty = 0.2$ mag (the median of S82 distribution in MacLeod et al. (2010)). Fig. 7 shows an example simulated DRW for SDSS-PS1-LSST.

To the simulated true DRW signal we add Gaussian noise corresponding to epochal heteroscedastic errors (eg. for SDSS epochs we use SDSS errors, for PS1 epochs we use PS1 errors, etc). This noise causes the underlying signal to become less constrained for larger errors (eg. CRTS and PTF portion). We further found that inclusion of ZTF data for 2018 would not significantly

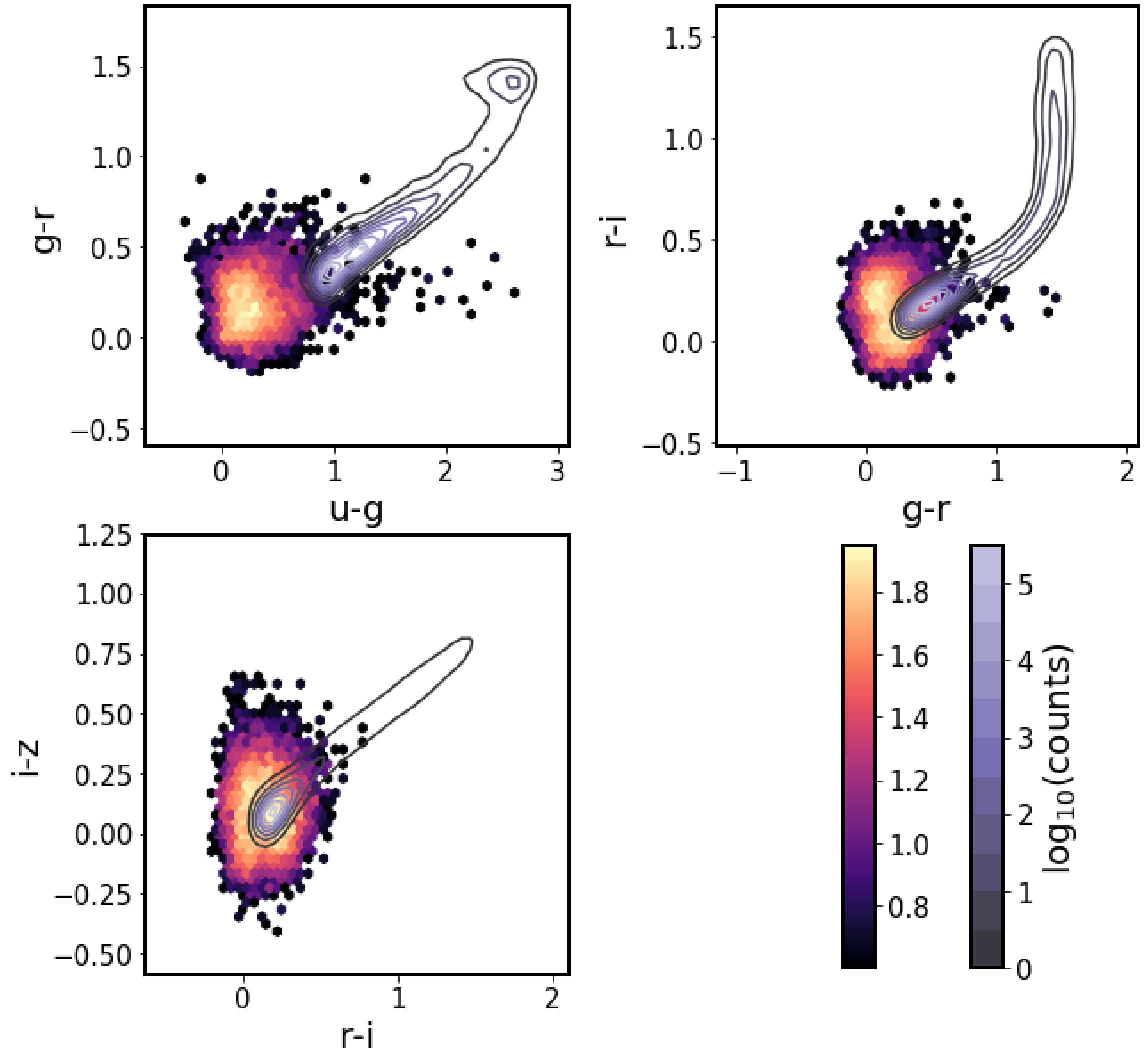

Figure 4. Regions occupied in color-color space by S82 quasars (colors) and standard stars (contours) (Schneider et al. 2010). We show only 10 000 randomly chosen stars from the full 1 mln + standard stars catalog Ivezić et al. 2007.

change our results. Inclusion of PS1 data with its excellent photometric uncertainty (as compared to ZTF or PTF) is the best improvement over existing SDSS results. We predict that in the future (after more data has been assembled and re-calibrated) ZTF will help, but not as dramatically as LSST (see Fig. 9). For this reason we found that using only SDSS-PS1 portion is the best tradeoff between adding more baseline vs introducing more uncertainty by noisy simulation - see Fig. 8 for error distribution, and Fig. 7 for illustration of the simulated light curve.

In accordance with Fig. 1, we find that extending the baseline decreases the bias in retrieved DRW parameters. Indeed, Fig. 9 shows that for an ensemble of 6444 simulated light curves the recovered DRW parameters become less biased when supplementing the SDSS data with PS1. , and th and 10

5. RESULTS: FITTING SDSS-PS1 WITH CELERITE

Given the results of simulations, we use combined SDSS-r and PS1 g,r,i data, bringing PS1 into common photometric filter of SDSS r.

Using just the SDSS r-band data our results of fitting the DRW with Celerite are consistent with MacLeod et al. (2011). On Fig. 11 we plot σ and τ for SDSS r-band fitted with Celerite, and the SDSS r-band only as fitted by MacLeod et al. (2011). The distributions are centered around 0, making Celerite results consistent with those of MacLeod et al. (2011). We also plot the distributions of τ to SF_{∞} on Fig. 12

5.1. *Trends with Rest-frame Wavelength*

Following MacLeod et al. (2011) , we shift all timescales to rest-frame, and prior to looking for cor-

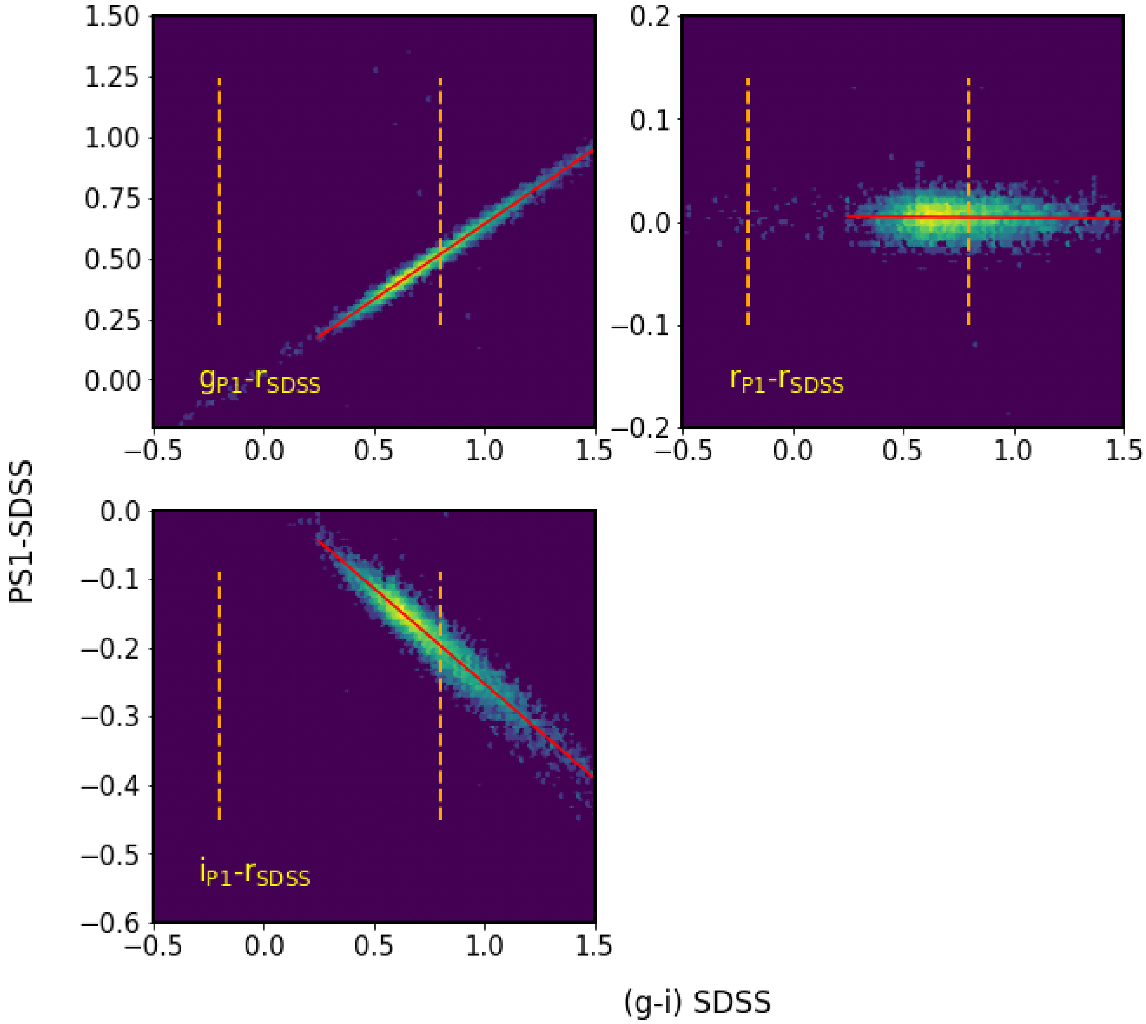

Figure 5. The SDSS-PS1 offsets. We plot only bright stars that have SDSS(r) ¡ 19, and that fulfill mErr * sqrt(Nobs) ¡ 0.03 . Each panel plots about 6000 stars of the 47000 CRTS S82 stars . Vertical dashed lines mark the region in SDSS color space occupied by quasars (see Fig. 4), used to fit the stellar locus with a polynomial.

relations with physical quantities (black hole mass, luminosities, redshifts), we correct all quantities to rest frame wavelength of $4000\mathring{A}$. This is because originally the SDSS data employed by MacLeod et al. (2011) were taken in near-simultaneous ugriz filters, each centered on different observers wavelength. Because quasars are not all at the same distance, this means that the same band would probe a different rest-frame wavelength for each quasar. MacLeod et al. (2011) found that τ_{RF} and SF_{∞} (f) can be connected to rest-frame wavelength λ_{RF} via power law :

$$f \propto \left(\frac{\lambda_{RF}}{4000\mathring{A}}\right)^{B} \tag{14}$$

Fig. 13 shows that both using SDSS and SDSS-PS1 the timescales and asymptotic amplitudes follow approximate power law coefficients found by MacLeod et al. (2011).

5.2. *Trends with Luminosity, Black Hole Mass, and Redshift*

Here we examine the main scientific results : the correlations between variability parameters $(\tau, SF\infty)$, and the physical properties of quasars (rest-frame wavelength λ_{RF}, redshift z, absolute i-band magnitude M_i, and black hole mass M_{BH}).

First, we consider the selection effects that are inherent to the quasar distribution. Fig. 14 shows the distribution of quasars as a function of redshift z, i magnitude M_i, and black hole mass M_{BH}. For instance, the trend of increasing redshift with M_i on the upper left panel is due to the fact that quasars have to be brighter to be included in the survey at increasing distances.

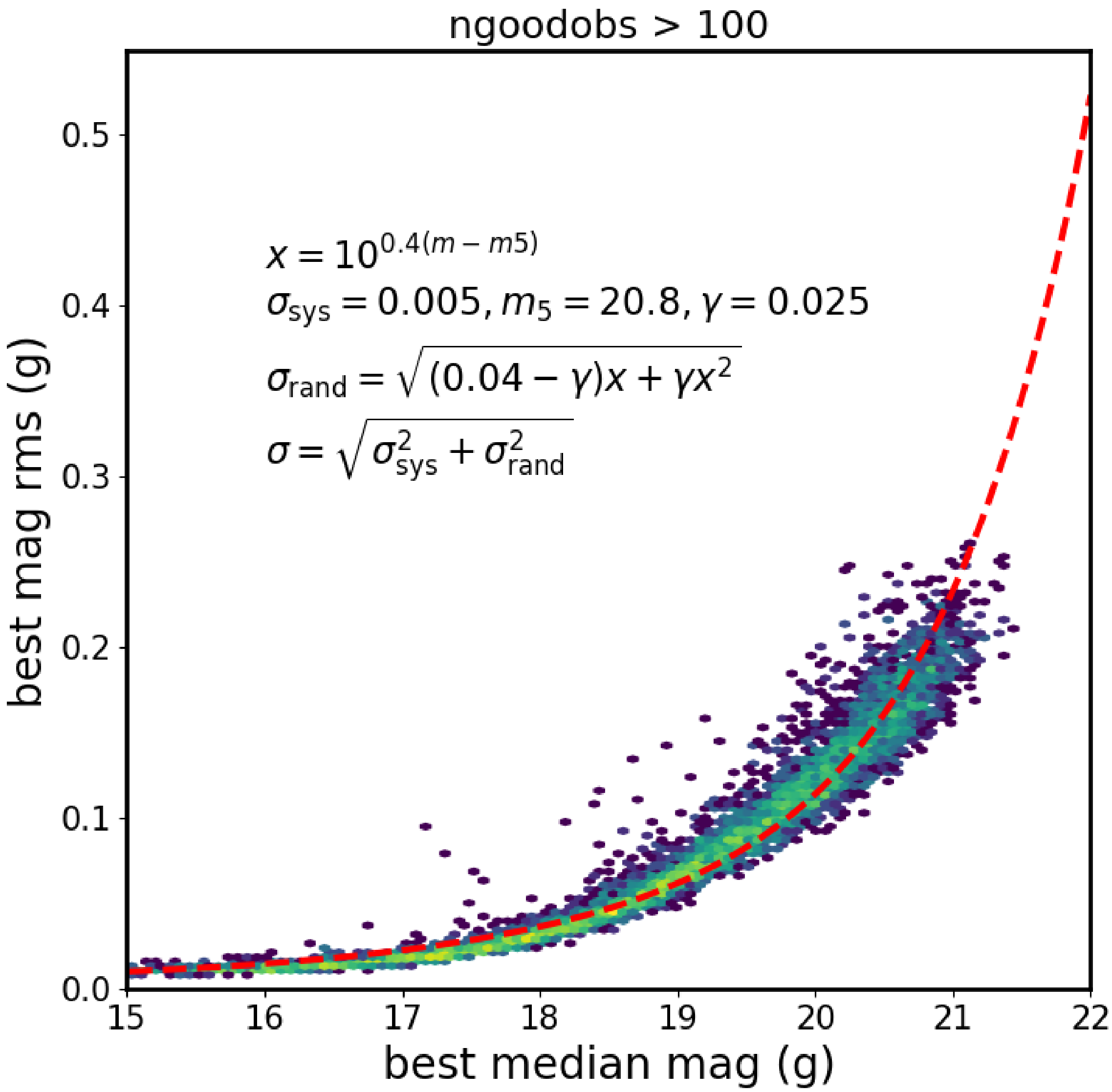

Figure 6. The rms spread as a function of magnitude for ZTF objects with over 100 observations. We overplot the functional describing the adopted error model. Properties of ZTF photometric uncertainty are largely similar to the PTF uncertainties.

On Fig. 15 τ and SF_∞ are shown as a function of absolute magnitude M_i, redshift z, and black hole mass M_{BH}.

We investigate these correlations by fitting a power law, after MacLeod et al. (2011) :

$$\log_{10} f = A + B\log_{10}\left(\lambda_{RF}/4000\text{Å}\right) + C(M_i + 23) + D\log_{10}\left(M_{BH}/10^9 M_\odot\right) \quad (15)$$

where f is τ_{RF} or SF_∞.

MacLeod et al. (2011) used the Shen2008 catalog, and k-corrected the absolute i-band magnitude to a redshift of 0. Since then, given that the redshift distribution of quasars peaks at z=2, it has become a more standard practice to k-correct absolute quasar magnitudes to z=2, as it is in Shen2011 catalog. We opt to use Shen2011 catalog as a source of physical quasar parameters.

Since MacLeod et al. (2011) used independently fitted each of five SDSS bands, the coefficients A,C,D,E were band-averaged. The result of that, using the new data of Shen2011, is shown on Fig. 16

Since we use SDSS-PS1 combined r-band data, we compare the new DRW parameters to results of fitting MacLeod et al. (2011) r-band only data (green line from Fig. 16). The comparison of new results against old ones is shown on Fig. 17

Since the simulations showed that we do decrease the bias by extending the baseline, we use the combined SDSS-PS1 light curves and show the space occupied by

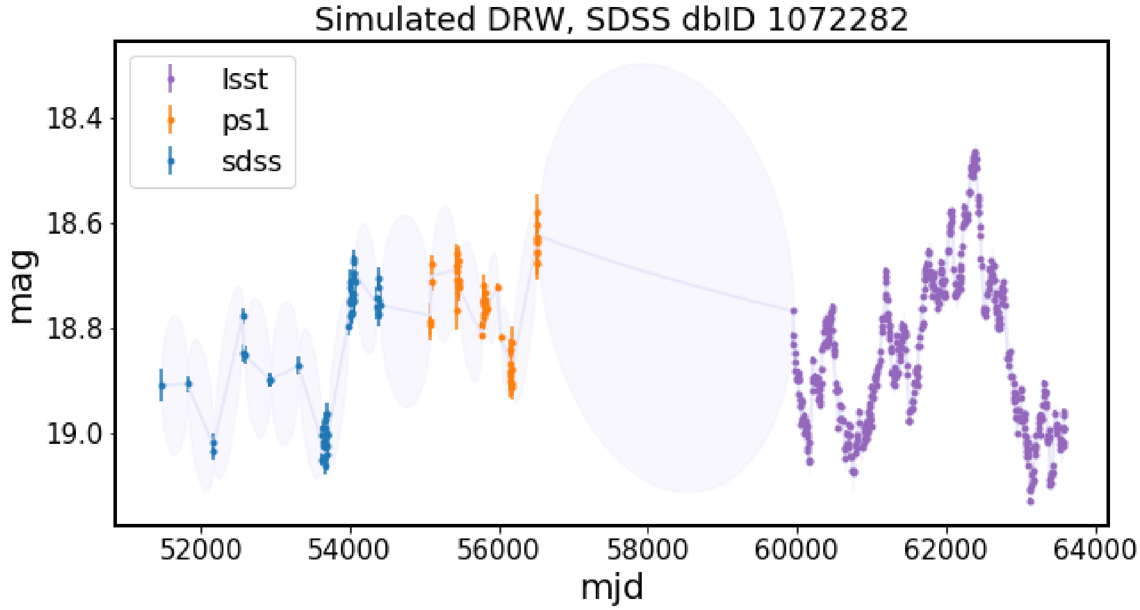

Figure 7. Simulated DRW process sampled at real cadence of SDSS, PS1, and simulated cadence of LSST. To each observed point we add Gaussian noise corresponding to the reported heteroscedastic (different for all points) errors for SDSS-PS1, and simulated magnitude-dependent errors for LSST.

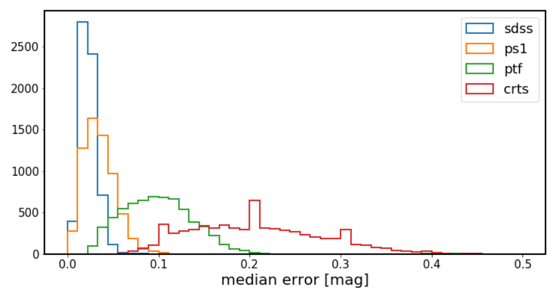

Figure 8. Distribution of median errors in combined r-band real light curves. We calculate the median per segment. This shows that the CRTS and PTF portions have much larger errors than SDSS, PS1, and are therefore less useful in improving the DRW parameters. This is the reason for using only SDSS-PS1 portion.

quasars in $SF_{\infty} - \tau - \sigma$ space, which confirms the results of MacLeod et al. (2011) (Fig. 18)

REFERENCES

AlSayyad, Y. 2016, PhD thesis, University of Washington. http://hdl.handle.net/1773/37020

Annis, J., Soares-Santos, M., Strauss, M. A., et al. 2014, ApJ, 794, 120, doi: 10.1088/0004-637X/794/2/120

Bauer, A., Baltay, C., Coppi, P., et al. 2009, ApJ, 696, 1241, doi: 10.1088/0004-637X/696/2/1241

Chambers, K. C. 2011, in Bulletin of the American Astronomical Society, Vol. 43, American Astronomical Society Meeting Abstracts #218, 113.01

Dexter, J., & Agol, E. 2011, ApJL, 727, L24, doi: 10.1088/2041-8205/727/1/L24

Dexter, J., & Begelman, M. C. 2019, MNRAS, 483, L17, doi: 10.1093/mnrasl/sly213

Drake, A. J., Djorgovski, S. G., Mahabal, A., et al. 2009, ApJ, 696, 870, doi: 10.1088/0004-637X/696/1/870

Flewelling, H. 2018, in American Astronomical Society Meeting Abstracts, Vol. 231, American Astronomical Society Meeting Abstracts 231, 436.01

Foreman-Mackey, D., Agol, E., Angus, R., & Ambikasaran, S. 2017, ArXiv e-prints. https://arxiv.org/abs/1703.09710

Graham, M. J., Djorgovski, S. G., Stern, D., et al. 2015, Nature, 518, 74, doi: 10.1038/nature14143

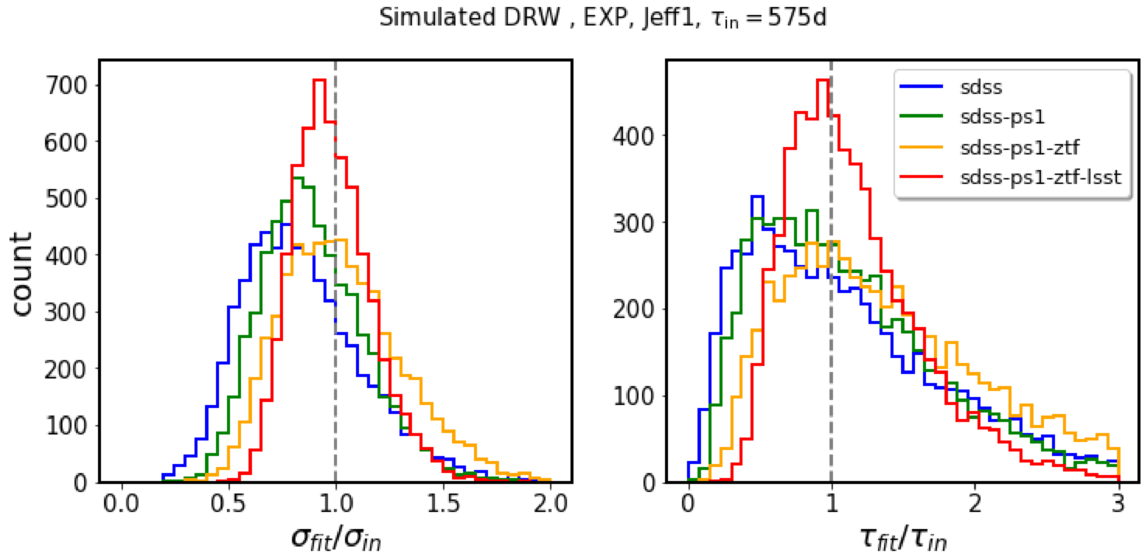

Figure 9. Retrieved τ and σ parameters for simulated LCs.

Hernitschek, N., Schlafly, E. F., Sesar, B., et al. 2016, The Astrophysical Journal, 817, 73

Ivezić, Ž., Smith, J. A., Miknaitis, G., et al. 2007, AJ, 134, 973, doi: 10.1086/519976

Kasliwal, V. P., Vogeley, M. S., & Richards, G. T. 2015, MNRAS, 451, 4328, doi: 10.1093/mnras/stv1230

Kelly, B. C., Bechtold, J., & Siemiginowska, A. 2009, The Astrophysical Journal, 698, 895

Kelly, B. C., Treu, T., Malkan, M., Pancoast, A., & Woo, J.-H. 2013, ApJ, 779, 187, doi: 10.1088/0004-637X/779/2/187

Kozłowski, S., Kochanek, C. S., Udalski, A., et al. 2010, ApJ, 708, 927

Kozłowski, Szymon. 2017, A&A, 597, A128, doi: 10.1051/0004-6361/201629890

LSST Science Collaboration, Abell, P. A., Allison, J., et al. 2009, arXiv e-prints, arXiv:0912.0201. https://arxiv.org/abs/0912.0201

MacLeod, C. L., Ivezić, Ž., Kochanek, C. S., et al. 2010, The Astrophysical Journal, 721, 1014

MacLeod, C. L., Brooks, K., Ivezić, Ž., et al. 2011, The Astrophysical Journal, 728, 26

MacLeod, C. L., Ivezić, Ž., Sesar, B., et al. 2012, The Astrophysical Journal, 753, 106

McGreer, I. D., Fan, X., Jiang, L., & Cai, Z. 2018, AJ, 155, 131, doi: 10.3847/1538-3881/aaaab4

McGreer, I. D., Jiang, L., Fan, X., et al. 2013, ApJ, 768, 105, doi: 10.1088/0004-637X/768/2/105

Palanque-Delabrouille, N., Magneville, C., Yèche, C., et al. 2013, A&A, 551, A29, doi: 10.1051/0004-6361/201220379

Rau, A., Kulkarni, S. R., Law, N. M., et al. 2009, PASP, 121, 1334, doi: 10.1086/605911

Ross, N. P., McGreer, I. D., White, M., et al. 2013, ApJ, 773, doi: 10.1088/0004-637X/773/1/14

Rybicki, G. B., & Press, W. H. 1992, ApJ, 398, 169, doi: 10.1086/171845

Schneider, D. P., Hall, P. B., Richards, G. T., et al. 2008, VizieR Online Data Catalog, 7252

Schneider, D. P., Richards, G. T., Hall, P. B., et al. 2010, VizieR Online Data Catalog, 7260

Sesar, B., Ivezić, Ž., Lupton, R. H., et al. 2007, AJ, 134, 2236

Tonry, J. L., Stubbs, C. W., Lykke, K. R., et al. 2012, ApJ, 750, 99, doi: 10.1088/0004-637X/750/2/99

Yang, J., Fan, X., Wu, X.-B., et al. 2017, AJ, 153, 184, doi: 10.3847/1538-3881/aa6577

Zu, Y., Kochanek, C. S., & Peterson, B. M. 2011, ApJ, 735, 80

Table 1. Color terms (offsets) between the following survey filters and SDSS(r) band, using the mean SDSS(g-i) color, so that the synthetic SDSS(r) magnitude can be found as $r_{SDSS,synth} = x - B_0 - B_1 SDSS(g-i)$

Band (x)	B_0	B_1
CRTS V	-0.0464	-0.0128
PTF g	-0.0294	0.6404
PTF R	0.0058	-0.1019
PS1 g	0.0194	0.6207
PS1 r	0.0057	-0.0014
PS1 i	0.0247	-0.2765

NOTE—To derive the offsets we used SDSS S82 1 mln standard stars catalog (Ivezić et al. 2007). We randomly selected 10% of that catalog, for which 48250 have CRTS light curves with at least 10 observations (B.Sesar). For these stars we obtained PS1 photometry from MAST http://panstarrs.stsci.edu and PTF from IRSA PTF Object Catalog https://irsa.ipac.caltech.edu/. We further imposed quality cuts requiring that the stars are bright: $r < 19$.

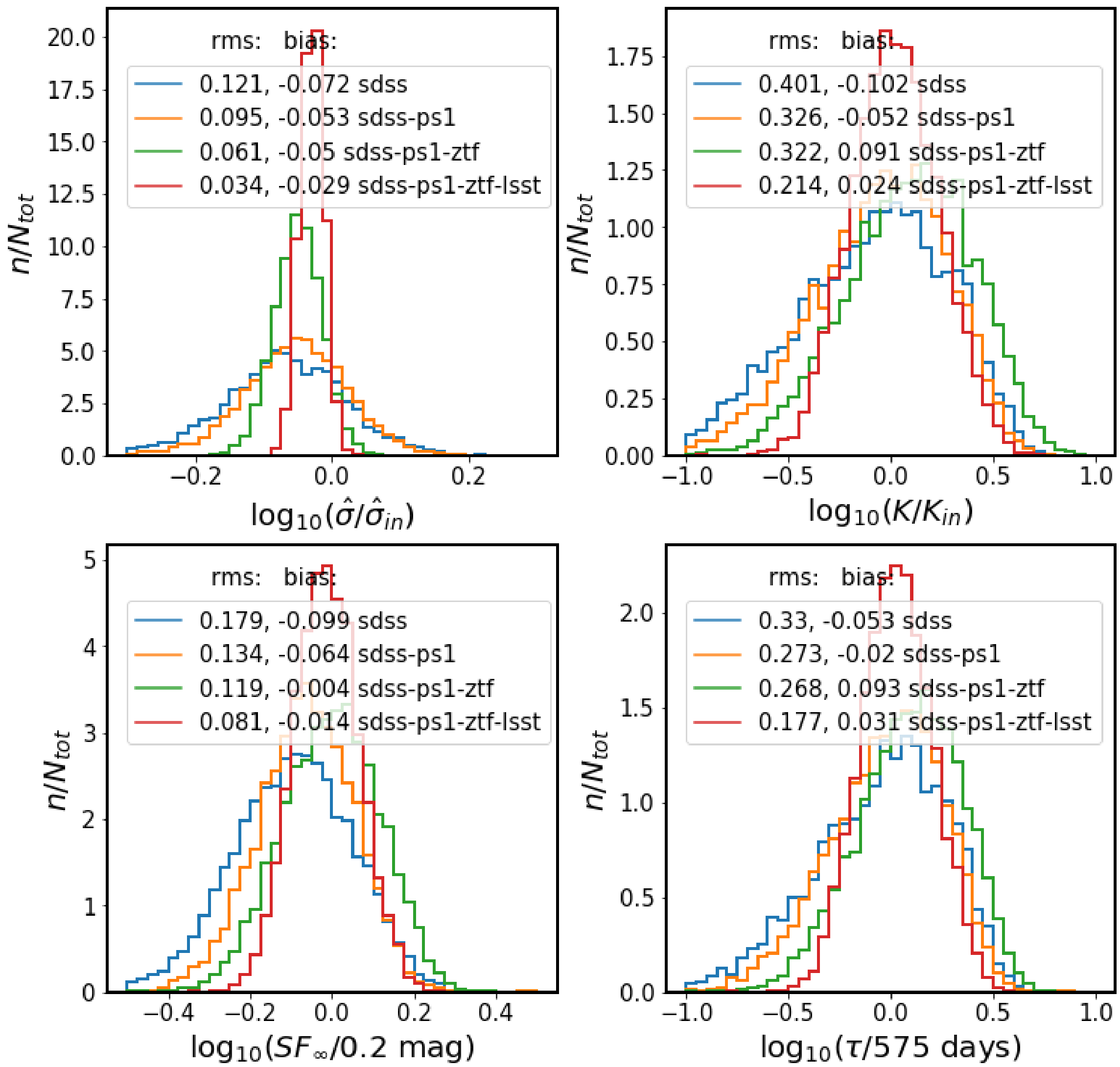

Figure 10. Comparison of retrieved parameters in relation to input parameters, shown as Fig.18 in MacLeod et al. (2011)

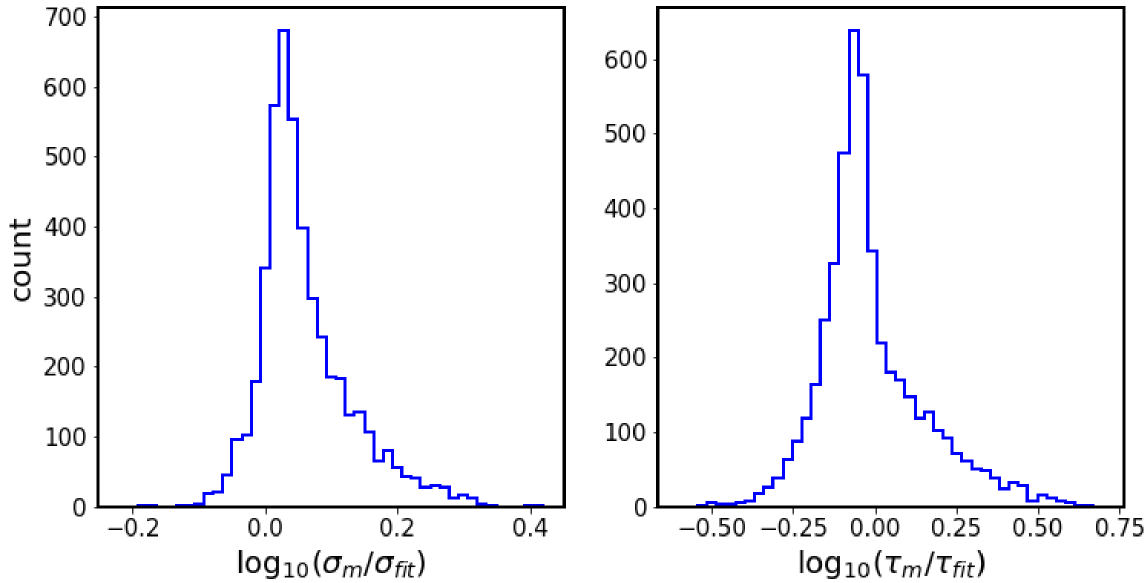

Figure 11. Plot comparing results for SDSS r-band fitting of MacLeod et al. (2011) (σ_m, τ_m), and current results for SDSS r-band using Celerite $(\sigma_{fit}, \tau_{fit})$.

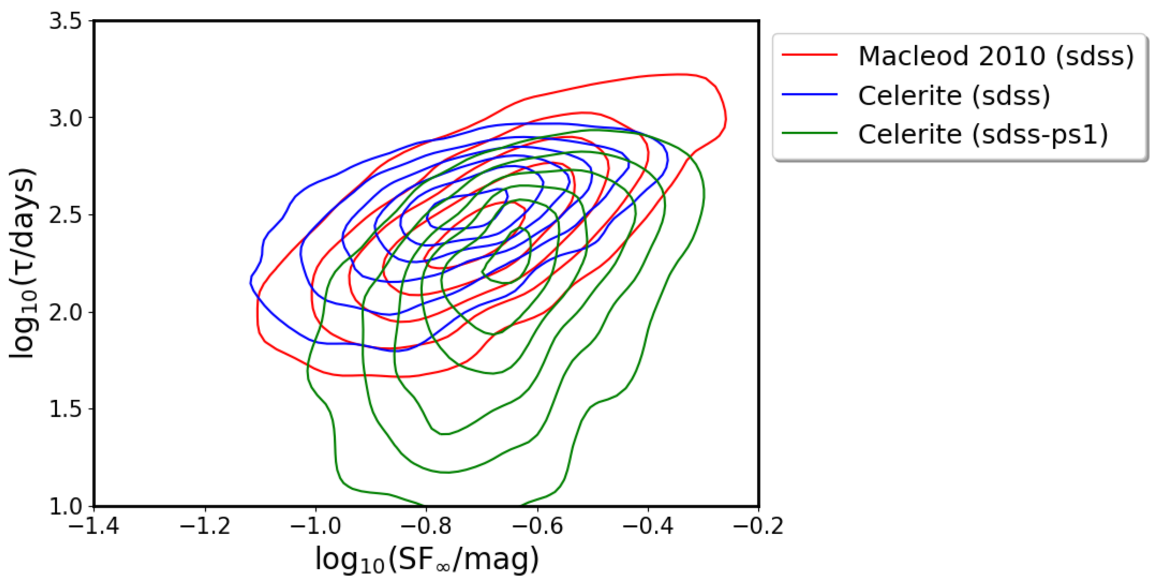

Figure 12. Comparing the rest-frame timescales τ, and asymptotic variability amplitudes SF_∞, for MacLeod et al. (2011) SDSS r-band, and combined SDSS and PS1 data.

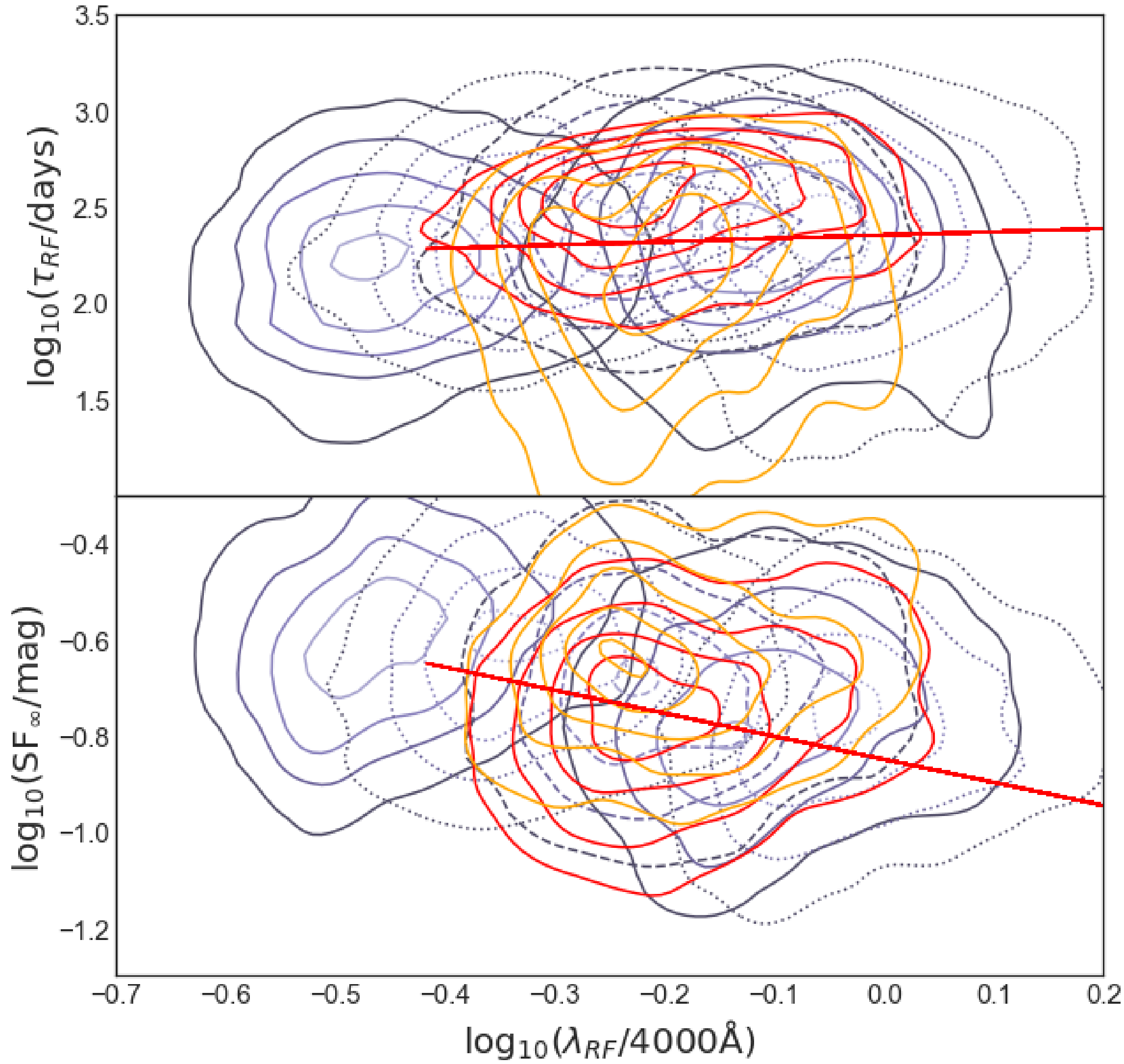

Figure 13. Rest-frame timescale τ (top panel), and long-term structure function SF_∞ (bottom panel), as a function of rest-frame wavelength λ_{RF}. The background contours show MacLeod et al. (2011) SDSS ugriz data, and the foreground contours denote the SDSS (red) and SDSS-PS1 (orange) new results with Celerite. In all datasets the quasars were selected according to criteria of MacLeod et al. (2011). The red line indicates the best-fit power law to MacLeod et al. (2011) data, with $B = 0.17$ an -0.479 for τ_{RF}, and SF_∞, respectively.

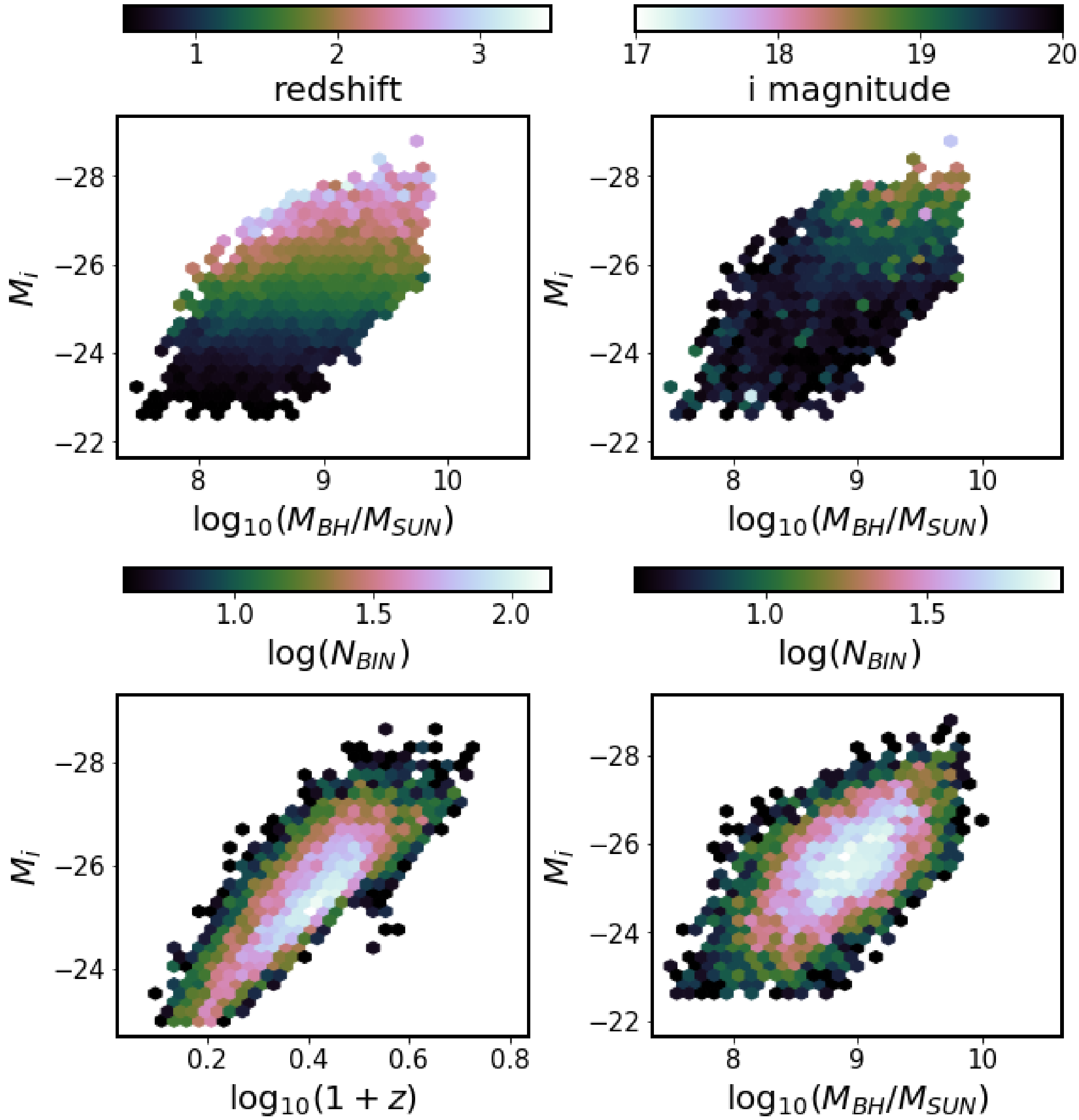

Figure 14. Distribution of quasars as a function of redshift, i magnitude, absolute i magnitude, and black hole mass.

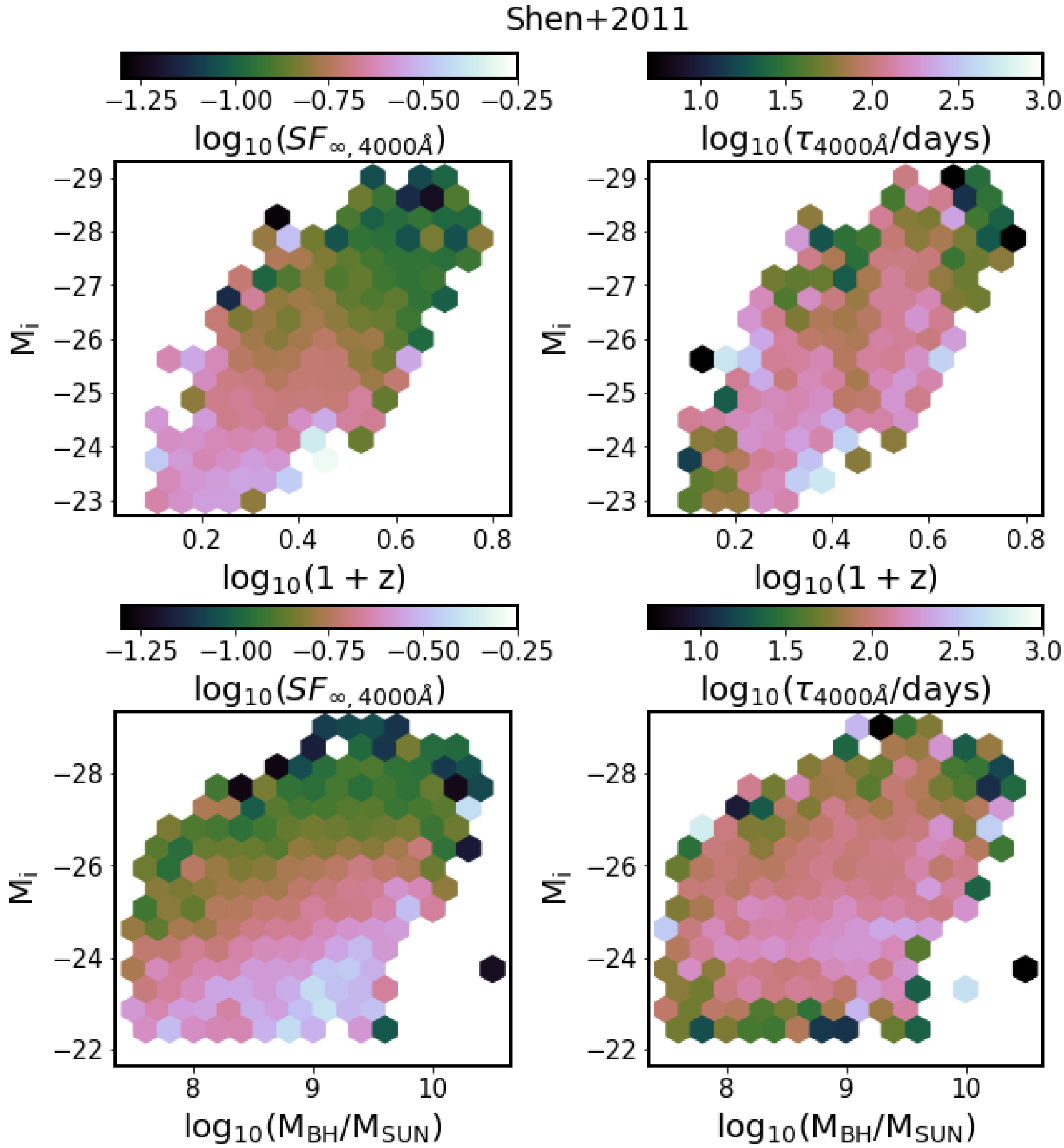

Figure 15. Long-term variability (SF_∞), and characteristic timescale (τ).

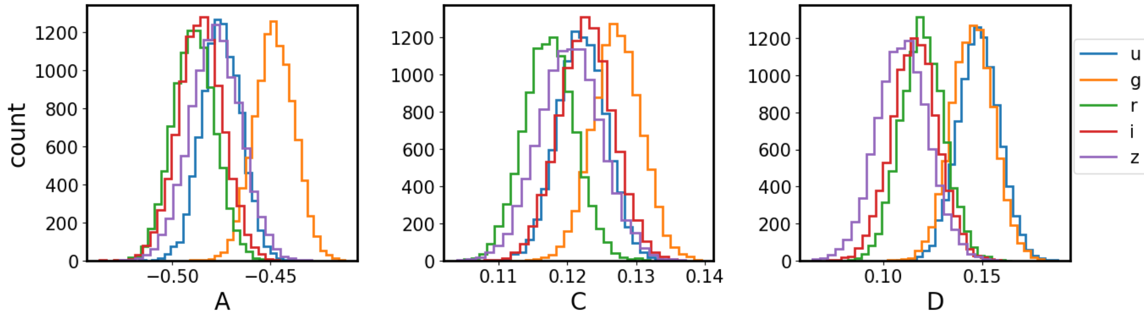

Figure 16. Samples from posterior MCMC draws for fit coefficients A,C,D (setting E=0), using Shen2011 values for redshift, absolute i-band magnitide, black hole mass. The vertical dashed line marks the band-averaged values for fit coefficients.

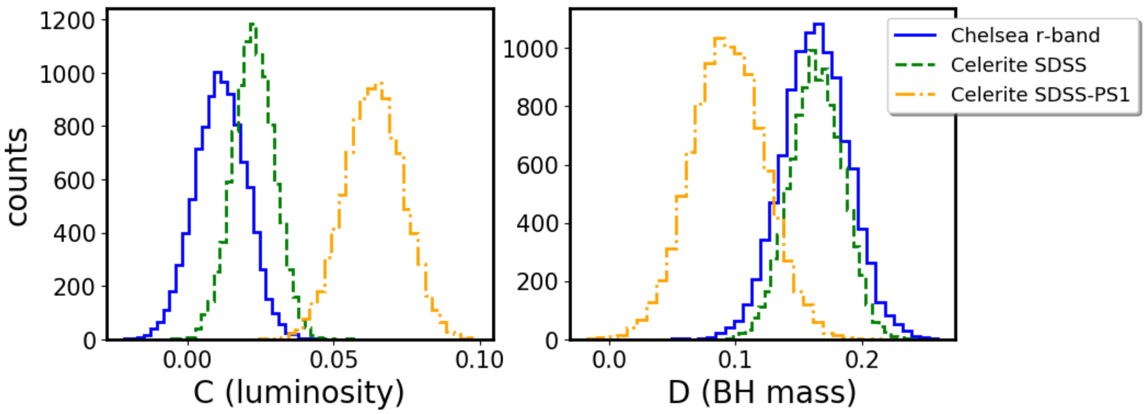

Figure 17. Comparison of Celerite fits of SDSS, SDSS-PS1 portions of combined quasar light curves against MacLeod et al. (2011) results of SDSS r-band only. The results from SDSS-only portion are consistent with previous results, and inclusion of the PS1 portion that increases the baseline decreases the timescale dependence on black hole mass, but increases the luminosity dependence. This can be understood as a rotation of the plane in (τ, M_i, M_{BH}) coordinates.

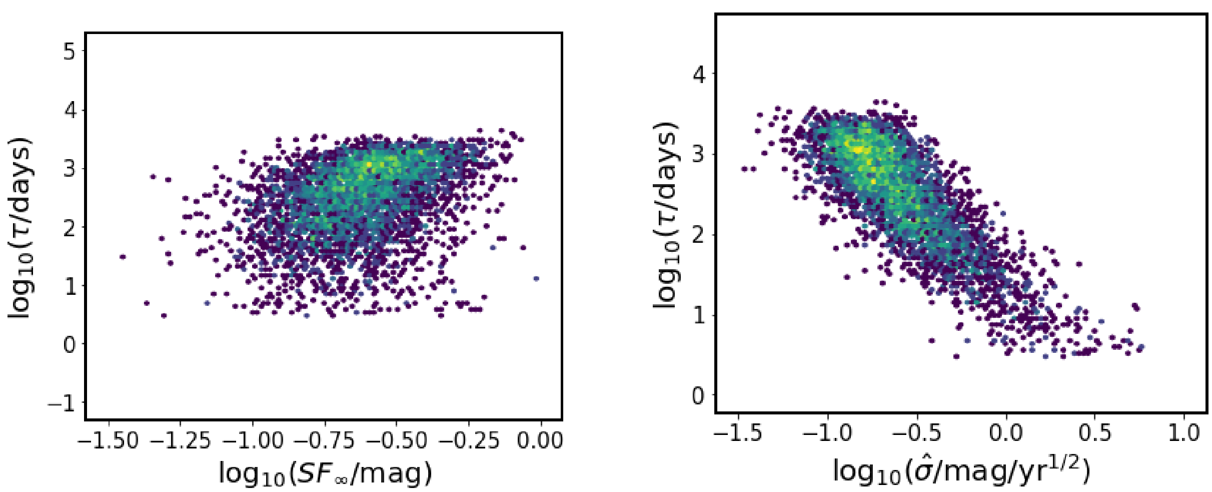

Figure 18. Both relations are shown in the observed frame. The left panel is like Fig.6, and the right like Fig.14 in MacLeod et al. (2011).